ADVANCED FUNCTIONAL MATERIALS
www.afm-journal.de

Hierarchically Assembled Counter Electrode for Fiber Solar Cell Showing Record Power Conversion Efficiency

Xinyue Kang, Zhengfeng Zhu, Tiancheng Zhao, Weijie Zhai, Jianchen Xu, Zhengmeng Lin, Kaiwen Zeng, Bingjie Wang, Xuemei Sun, Peining Chen, and Huisheng Peng**

Fiber solar cells have attracted significant interest as a promising wearable power supply solution for their merits of high flexibility, lightweight, and good compatibility with textile configuration and weaving process. However, because of the limited ion diffusion and charge transfer in the fiber counter electrode, the poor photovoltaic performances have long been one obstacle to hinder their real applications. Herein, in mimicking the efficient mass transport and exchange through the vascular tissue of plants like pine needle, a hierarchically assembled carbon nanotube (HCNT) fiber counter electrode is fabricated by a scalable process. The designed hierarchically aligned channels with large sizes of micrometers and small sizes of tens of nanometers in the HCNT fiber offers high-flux pathways for rapid ion diffusion and abundant active area for charge transport, thus endowing the fiber dye-sensitized solar cell with a record power conversion efficiency of 11.94%. By weaving such fiber solar cells in a scalable way, a flexible and breathable large photovoltaic textile (17 cm × 22 cm) is made to present a power output of 22.7 mW. These fiber solar cells are further integrated with fiber lithium-ion batteries to efficiently power wearable electronics.

1. Introduction

In the past decade, the emerging technologies of the Internet of Things have boosted the development of wearable electronics, and brought about urgent demands on portable and mobile power supplies.[1–4] Wearable photovoltaics (PVs) are attractable for providing a sustainable power supply by converting clean and high-quantity solar energy into electricity.[5–9] They generally exhibit superior power output compared with other wearable energy-harvesting devices such as triboelectric, piezoelectric devices, and biofuel cells.[10] Among them, the fiber solar cells with the merits of lightweight, flexibility, and compatibility with complex and irregular substrates, have become promising candidates for wearable energy supplies.[11–14] Among them, fiber dye-sensitized solar cells (FDSSCs) have attracted extensive interest from both academia and industry due to their both low toxicity and cost.[15–17] However, the unsatisfactory power conversion efficiencies (PCEs, typically less than 10%) as well as unscalable production have critically hindered their practical applications.

Fiber counter electrodes are critical to the PCE of FDSSC by catalyzing redox couples in the electrolyte. Pt is an extensively used counter electrode with high catalytic activity, but it suffers from the limits like high cost, scarce reserve, and low specific surface areas especially in the form of Pt wires.[18] Afterward, many other catalytic materials like transition metal compounds[19,20] and conductive polymers[21] had been widely explored as alternative counter electrodes, but they were usually grown/coated on conductive wires with lower activity. Some works used carbon nanotube fibers as counter electrodes and modified their surface by hydrophilic treatment to enhance the loadings of active components.[22] But, their densely arranged arrays at the nanoscale generally restrain the ions of the electrolyte from diffusing inwards to the deeper region. This is unfavorable for the efficient mass transport of redox couples as well as charge transfer at the counter electrode, thus resulting in inferior catalytic performances.[23] This problem became particularly serious in cobalt-based redox systems for the slow mass transport retarded by large-size Co^{2+}/Co^{3+} redox couples.[24] Consequently, highly efficient Co-mediated FDSSCs have not been reported yet, even though they can theoretically achieve high PCEs owing to their intrinsic low voltage losses.[25] Moreover, the high cost and unscalable hydrothermal method for fiber electrodes further prevented their large-scale applications. Hence, obtaining large-scale fiber counter electrodes with high catalytic activity remains an unmet need.

In nature, vascular tissues in plants display inherent hierarchical channel structure which is critical for efficient mass transport and exchange among cells. For instance, viminous pine needles demonstrate internal vascular tissues with both main and branch veins at millimeters and micrometers (**Figure 1**a). The main veins with millimeter-scale channels offer high-flux pathways for rapid transport of water and sucrose,

X. Kang, Z. Zhu, T. Zhao, W. Zhai, J. Xu, Z. Lin, K. Zeng, B. Wang, X. Sun, P. Chen, H. Peng
State Key Laboratory of Molecular Engineering of Polymers
Department of Macromolecular Science and Laboratory of Advanced Materials
Fudan University
Shanghai 200438, China
E-mail: peiningc@fudan.edu.cn; penghs@fudan.edu.cn
The ORCID identification number(s) for the author(s) of this article can be found under https://doi.org/10.1002/adfm.202207763.

DOI: 10.1002/adfm.202207763

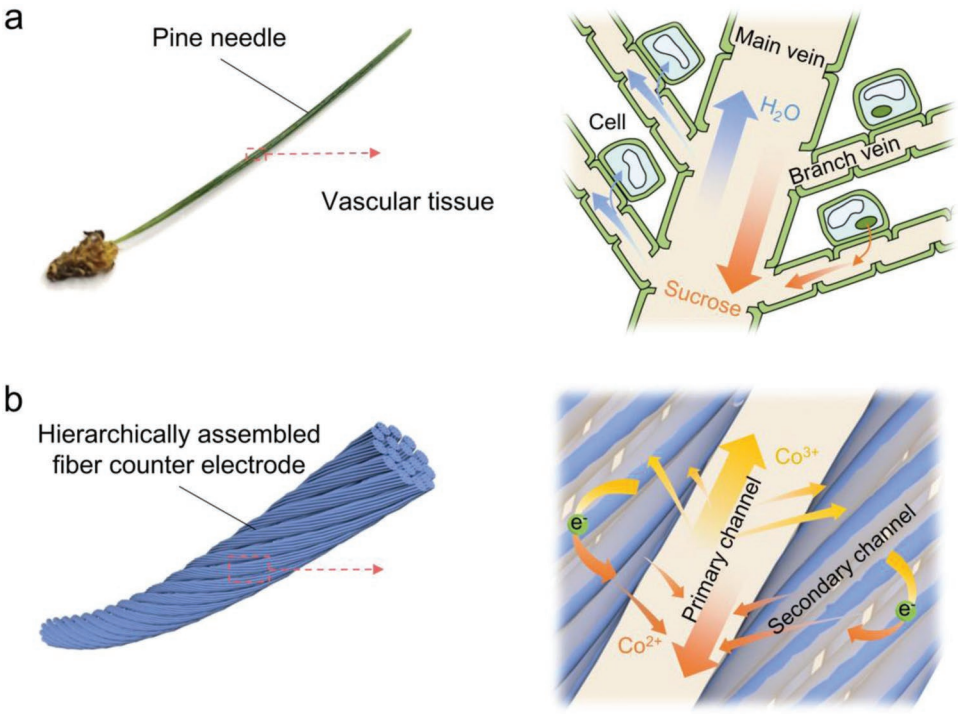

Figure 1. Structures of pine needle and HCNT fiber counter electrode. a) Photograph (left) of a pine needle and scheme (right) showing mass delivery through the hierarchical vascular tissue in the pine needle. b) Schemes of the HCNT fiber (left) and enlarged view of hierarchical channels for rapid ion diffusion and charge transport (right).

while the micrometer-scale branch veins guarantee sufficient areas for material exchange. We hypothesize if a hierarchical channel structure is introduced into fiber counter electrodes, it is possible to effectively promote ion transport and charge exchange, thus presenting high catalytic activity.

In this study, we design such a fiber counter electrode with hierarchical channel structure by assembling carbon nanotubes into fiber with both high mechanical strength, and electrical conductivity.[26–30] The hierarchically assembled carbon nanotube (HCNT) fiber counter electrode (Figure 1b) was prepared through a scalable process including floating catalyst chemical vapor deposition, twisting treatment and electrodeposition of Pt nanoparticles. The abundant primary and secondary channels at micrometer and nanometer scales were achieved to favor ion diffusion and charge transfer, greatly improving effective areas for electrochemical reaction. Additionally, electrodepositing highly active Pt nanoparticles further enhanced the catalytic activity of HCNTs. With the above fiber counter electrode, the fabricated FDSSC composed of Y123-sensitized Ti/TiO_2 photoanode and Co-based electrolyte produced a record PCE of 11.94%. The FDSSC was further woven into a photovoltaic textile with size of 17 cm × 22 cm and integrated with fiber batteries to power wearable electronic devices.

2. Results and Discussion

In brief, the HCNT@Pt fiber was prepared by three steps (**Figure 2**a). First, a primary carbon nanotube (CNT) fiber with diameter of ≈40 µm was continuously synthesized by floating chemical vapor deposition, in which abundant nanochannels were generated (Figure 2e). Their sizes ranged from several to tens of nanometers (Figure S1, Supporting Information). Subsequently, the HCNT fiber with a diameter of 150 µm (Figure 2c) was achieved by twisting a bundle of primary CNT fibers to form helical micrometer-scale channels (Figure 2f) among the primary fibers. The average size of these channels was 1.7 µm through the analysis of size statistical distribution (Figure S20b, Supporting Information). The detailed optimization of the microchannel size was described in the experimental section. Finally, the HCNT fiber was soaked in an electrolyte containing 1 mM K_2PtCl_6 and 0.1 M KCl to realize the electrodeposition of Pt nanoparticles. As shown in Figure 2d,g, Pt nanoparticles with an average size of ≈40 nm were uniformly deposited on the surface of the HCNT@Pt fiber. In this preparation process, primary CNT fibers can be obtained at kilometer scale (Figure S2, Supporting Information).

To investigate the effects of the hierarchical structures on the catalytic activity of fiber counter electrodes, a CNT fiber without microchannels (Figure S3, Supporting Information) and carbon fiber without nanochannels (Figure S4, Supporting Information) were prepared as control groups. All of them shared the similar diameter of ≈150 µm. The electrocatalytic activities of these fiber electrodes were evaluated by cyclic voltammetry (CV). The CV curves were measured in a three-electrode system using Pt as counter electrode, Ag/AgCl as reference electrode, and acetonitrile-solution contained Co^{2+}/Co^{3+} redox couples as electrolyte. As demonstrated in **Figure 3**a, one pair of oxidation and reduction peak was recorded in the CV curves, indicating a simple one-step reaction of the cobalt bipyridine redox

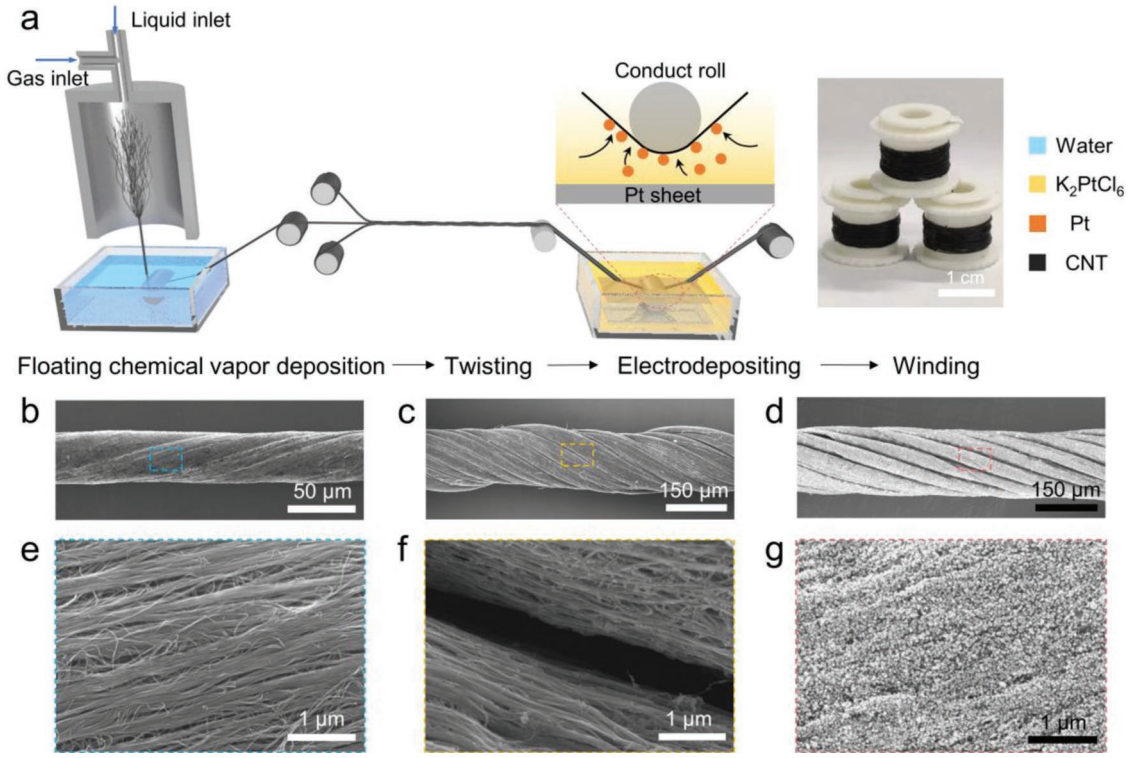

Figure 2. Preparation process and structure of the HCNT electrode. a) Schematic showing the setup to prepare HCNT fiber (left) and photograph of three reels of HCNT fiber. b–d) SEM images of primary CNT fiber, HCNT fiber, and HCNT@Pt fiber, respectively. e–g) High-resolution SEM images in b–d), respectively.

couple.[31,32] Similar reduction peaks were located at ≈0.23 V for the HCNT fiber and CNT fiber, and no obvious redox peak was observed for the carbon fiber. The high peak current density in CV curves generally showed the counter electrode owned enhanced electrocatalytic activity to generate higher photocurrent.[33] As shown in Figure 3a, the peak current density of HCNT fiber was higher than that of CNT and carbon fibers, indicating the highest electrocatalytic activity for Co^{2+}/Co^{3+} redox couples in the HCNT fiber electrode. Such a high activity may be attributed to the largest normalized electrochemical active area of ≈2.31, which was twice of CNT fibers (1.16) and three times of carbon fibers (0.78) (Figure 3b). These normalized areas were calculated from the CV curves (Figure S5, Supporting Information), measured by three electrodes system in $K_4Fe(CN)_6$ and KCl solution.[34] The large active area was derived from the unique hierarchical channels in the HCNT fiber. On the one hand, the nanochannels of HCNT and CNT fiber provided higher specific surface areas and thus provided more reaction sites than that of carbon fiber.[35,36] On the other hand, microchannels promoted ions to diffuse deeper in the electrode and thus provided more interior surfaces for reaction.[37]

Electrochemical impedance spectroscopy (EIS) analysis was carried out to further evaluate the charge transfer and mass transport kinetics, by using the symmetrical cells fabricated by two identical counter electrodes and Co^{2+}/Co^{3+} electrolyte. As demonstrated in the Nyquist plots (Figure 3c), the intercept of the left semicircle on the x-axis represented the series resistance (R_S) reflecting the whole electrical conductivity of device. The diameters of the semicircles at high and low frequencies represent charge transfer resistance (R_{ct}) and Nernst diffusion resistance (Z_N), respectively. The EIS data were summarized in Table S1 (Supporting Information). Compared with carbon fiber, the CNT fiber and HCNT fiber showed much lower R_S, due to higher electrical conductivities than that of carbon fibers. For instance, the resistances for CNT, HCNT and carbon fibers were measured as 4.1, 4.3 and 24.9 Ω cm^{-1}, respectively. Additionally, compared with carbon fiber, the lower R_{ct} for HCNT (0.38 Ω cm^2) and CNT (0.44 Ω cm^2) fibers indicated their superior activities, which originated from the abundant reaction areas of HCNT and CNT with nanochannels. Moreover, compared with CNT fiber, the Z_N of HCNT fiber was much lower, indicating a reduced ion diffusion resistance by introduction of microchannels. These microchannels could shorten the ion diffusion distance from electrolyte to the electrode interior by acting as an electrolyte buffering reservoir[38] (Figure S6, Supporting Information). Overall, the hierarchical channels in the HCNT fiber could effectively improve the charge transfer and mass transport.

Based on the above characteristics, HCNT counter electrodes were beneficial to improve photovoltaic performance. Specifically, the low R_S and R_{ct} indicated good electrical conductivity and high electrochemical catalytic activity,[39] thus leading to a higher short-circuit current density (J_{SC}) of 18.26 mA cm^{-2} compared with CNT and carbon fibers. Additionally, the decreased Z_N represented rapid transport of reduced ions for facilitating dye regeneration, resulting in reduced charge recombination.[40] Thus the open-circuit voltage (V_{OC}) of HCNT was enhanced to 0.923 V, and the fill factor (FF) was increased to 0.66. Therefore,

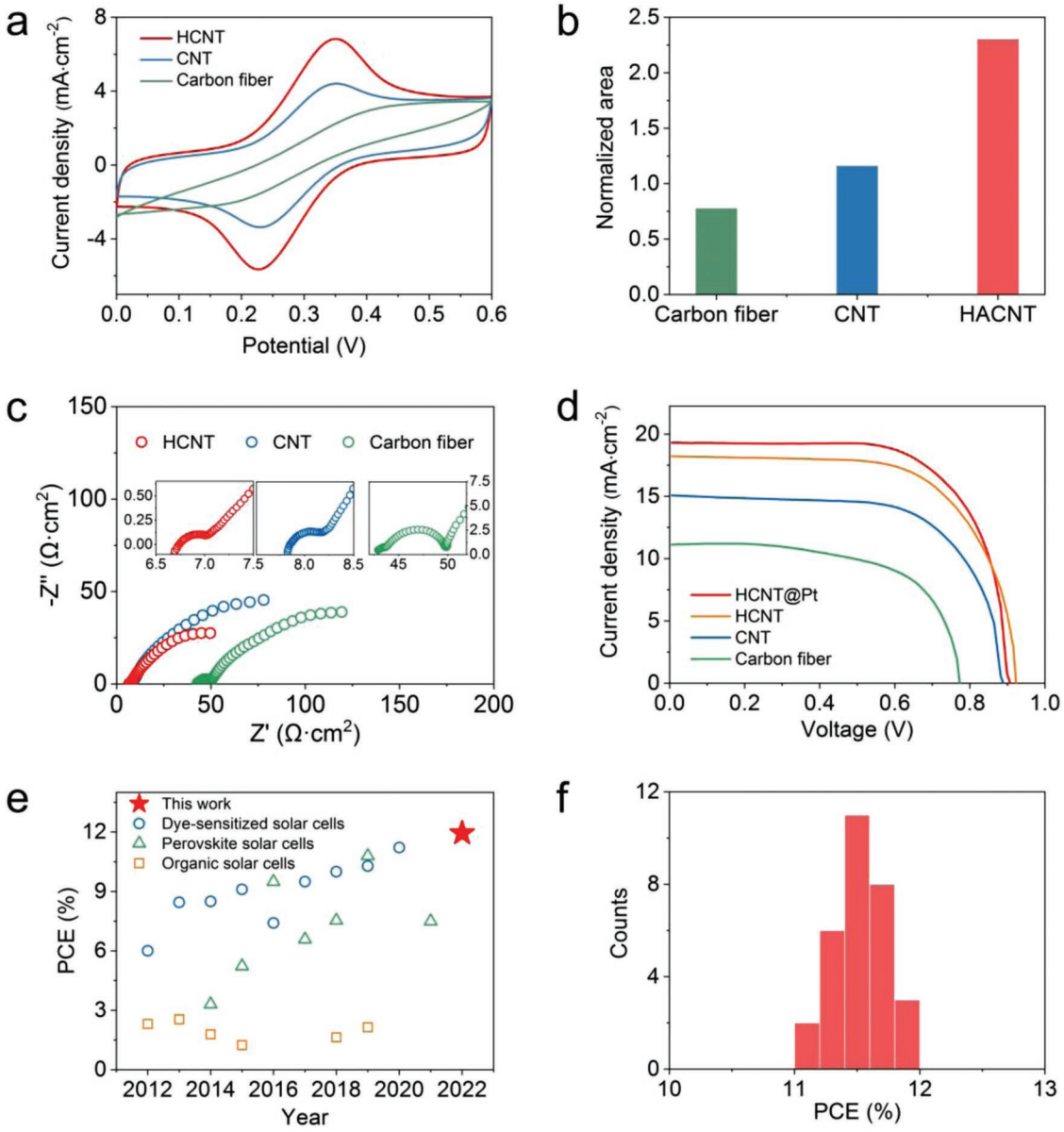

Figure 3. Photovoltaic performances and electrochemical characteristics of FDSSCs. a) CV curves of counter electrodes in the acetonitrile-solution containing 10 mM Co^{2+}, 1 mM Co^{3+} and 0.1 M $LiClO_4$. The scan rate was 50 mV s^{-1}. b) Normalized electrochemical active areas of counter electrodes measured in 20 mM $K_4Fe(CN)_6$ and 0.2 M KCl solution. The scan rate was 20 mV s^{-1}. c) Nyquist plots of symmetrical cells fabricated with two identical electrodes measured at 0 V from 100 kHz to 0.01 Hz in the acetonitrile solution containing 0.22 M Co^{2+}, 0.033 M Co^{3+}, 0.1 M $LiClO_4$ and 0.2 M 4-tert-butylpyridine. Inset: enlarged view of Nyquist plots at high frequency. d) *J-V* curves of the FDSSCs based on different counter electrodes with the same efficient area. e) Comparisons of the PCE of fiber solar cells to date. f) Statistics of the PCE distribution for 30 independently fabricated fiber FDDSCs. The average PCE was 11.51 ± 0.21%.

the FDSSCs based on HCNT electrodes exhibited higher PCE (11.14%) than CNT-based (8.89%) and carbon fiber-based (5.43%) FDSSCs. A PCE enhancement also occurred for N719-based FDSSC using HCNT as fiber counter electrode (Figure S7, Supporting Information). The current density versus voltage (*J-V*) curves were measured under an AM 1.5 illumination (Figure 3d), and the photovoltaic parameters are listed in Table S2 (Supporting Information). The structure and fabrication process of FDSSCs was detailed in Figure S8 (Supporting Information) and experimental section. Moreover, the PCE of HCNT-based FDSSCs could be further enhanced by depositing Pt nanoparticles. The photovoltaic performance of FDSSCs with different Pt loadings was shown in Table S3(Supporting Information). The optimum performance was achieved at a Pt loading of 4.24 mg cm^{-2}. As a result, the HCNT@Pt-based FDSSC exhibited a superior PCE of 11.94% (Figure 3d), a record among all fiber solar cells to date (Figure 3e and Table S4, Supporting Information). The TiO_2 nanotube arrays were widely used in fiber photoanode because their aligned nanostructures provided direct pathways for electron transport and large surface

areas for dye absorption,[41] and a maximal PCE of 11.22% had been reported for the resultant FDSSCs.[42] The achieved PCE of 11.94% in this work was lower than the highest theoretical PCE of 28% according to the Shockley-Queisser limit,[43] indicating it still had room for improvement. The incident photo-to-electron conversion efficiency (IPCE) spectra of HCNT@Pt based-FDSSC (Figure S9, Supporting Information) showed wide response range of 330–700 nm and high IPCE value of 85%. The deviation between the integrated J_{SC} from IPCE spectra and J_{SC} from J–V characterization was similar to previous reports.[17,44,45] In addition, the PCE statistics of 30 devices in Figure 3f indicated a stable performance due to the reproducibility of the fabricating method.

The underlying mechanism for the enhancement of the hierarchical structure was further investigated. The infiltration time of electrolyte was shortened (Table S5, Supporting Information) and the ion concentration within the HCNT was increased (Figure S10, Supporting Information) after introduction of microchannels, indicative of improved mass transport. The open-circuit voltage decay curves recorded in Figure S11 (Supporting Information) indicated reduced charge recombination for HCNT-based FDSSC. Additionally, the intrinsic nanostructure of HCNT provided a large number of reactive sites for charge transfer.[46] Therefore, the photovoltaic performances of FDSSCs were enhanced because the HCNT electrodes offered high-flux pathways for rapid ion diffusion and abundant active area for charge transport.

Our FDSSCs were mechanically robust and flexible to withstand various deformations. As shown in **Figure 4**a, the PCE was varied by less than 10% after the FDSSCs were repeatedly bent (1000 cycles with bending angle of 120°), twisted (with a pitch of 4 cm and curvature radius of 0.5 cm) and pressed (under 278 N m^{-2}). Due to the efficient encapsulation, the performances of FDSSCs under open air were similar to that under inert (Ar) atmosphere (Figure S12, Supporting Information). Also, the FDSSCs showed good stability to withstand humidity. The PCE was stably maintained (with a retention of 94%) under a humidity of 90% (Figure S13, Supporting Information). By weaving such FDSSCs, we had further made a flexible and breathable photovoltaic textile. Its V_{OC} and J_{SC} could be conveniently tuned by changing the number of FDSSCs connected in parallel (Figure S14, Supporting Information) and series (Figure S15, Supporting Information), according to the application requirements. Owing to the scalable production combined with excellent performances of fiber counter electrodes, a large textile of 17 cm × 22 cm (active area of 32 cm^2) was achieved to generate high V_{OC} of 5.055 V and J_{SC} of 7.483 mA under outdoor sunlight. Its maximum electricity output (P_{max}) was 22.7 mW under an illumination of AM 1.5G (Figure S16, Supporting Information), which is one to two orders of magnitude higher than other fiber solar cells (Figure 4b),[47–52] and can drive Bluetooth to work effectively. Moreover, the energy converted by solar cells could be timely stored in fiber lithium-ion batteries (FLIBs)[53] to realize a self-powered system with steady electricity output. For instance, the voltage of the FLIB recorded in Figure S17 (Supporting Information) showed that it was charged by FDSSCs from 3.1 to 4.2 V under the illumination of AM 1.5 and discharged to 2.5 V at a constant current of 0.5 mA.

For real application scenarios, we demonstrated a smart healthcare garment integrated with power-supplying textile that can power various wearable devices for real-time health monitoring and displaying (Figure 4c,d). As a proof-of-concept, a sweater woven with FDSSCs and FLIBs could charge wearable electronics like smart watch to monitor heart rate (Figure 4e), and the integrated textile display module[54] could visually demonstrate the heart rate status (Figure 4f). Additionally, the applications of the photovoltaic textile can be broadened by increasing its power output through enlarging its area and weaving density of FDSSCs. Based on the data measured above, it is expected that the P_{max} of FDSSCs will reach 1 W with an area of a piece of garment (≈0.15 m^2), which is enough to charge a variety of wearable electronic devices (200 μW to 1 W) and even cell phones.

3. Conclusion

In conclusion, inspired by vascular tissue in pine needles, we presented an HCNT fiber counter electrode with hierarchical channels, which showed both high electrocatalytic activity and transport kinetics. After assembly with Y123 sensitized Ti/TiO_2 photoanode and Co^{2+}/Co^{3+} redox couple, the resulting FDSSC exhibited a record PCE of 11.94%. Additionally, profiting from a scalable fabrication process, we produced a flexible photovoltaic textile with size of 17 cm × 22 cm that showed V_{OC} of 5 V and J_{SC} of 7 mA under outdoor sunlight. These fiber solar cells may be promising to power a variety of flexible and wearable electronics.

4. Experimental Section

Materials: Carbon fiber (W0S1009) was purchased from Taiwan Carbon Technology Co., Ltd. Ti wire (127 μm) was purchased from Alfa Aesar. Y123 and Co-based redox electrolyte (OPV-AN-C) was purchased from Yingkou OPV Tech New Energy Co., Ltd. $Co^{3+/2+}$ redox electrolyte was mainly composed of $Co(bpy)_3(ClO_4)_2$, $Co(bpy)_3(ClO_4)_3$, $KClO_4$, and 4-tert-butyl pyridine. $Co(bpy)_3(ClO_4)_2$ was synthesized by dissolving $CoCl_2{\cdot}6H_2O$ and polypyridine ligand in water at 50 °C for 1 h, and lithium perchlorate was added after cooling. Then, the precipitate was washed with water and methanol. $Co(bpy)_3(ClO_4)_3$ was formed by oxidating $Co(bpy)_3(ClO_4)_2$ with $NOBF_4$.[55] Dehydrated acetonitrile (99.0%) and tert-butanol (99.0%) were purchased from Sinopharm Chemical Reagent Co., Ltd. K_2PtCl_6 (99.9%), $K_4Fe(CN)_6$ (99.99%), and KCl (99.98%) were purchased from Aladdin.

Preparation of Counter Electrodes: CNT fibers were synthesized by floating catalyst chemical vapor deposition method. For the feed solution, ethanol was used as carbon resource, and selected ferrocene (1–3.5 wt.%) and thiophene (0.5–3.5 wt.%) served as the composite catalyst. The solution was bumped into a furnace at 1200–1300 °C in H_2 and Ar atmosphere at a feeding rate of 0.1–0.3 mL min^{-1}. The synthesized CNTs were then pulled out of the furnace, densified by water and ethanol solution, and dried to produce CNT fibers. Their diameters can be tuned by changing feeding speed and catalyst concentration. In this work, the diameter of 20, 40 and 60 μm were used as primary CNT fibers. Second, several bundles of primary CNT fibers were twisted together by a spinning machine to prepare HCNT fiber with diameter of 150 μm. The number of bundles of primary CNT was optimized below. The HCNT fibers consisting of 5, 15 and 30 bundles of primary CNT fibers were named HCNT-1, HCNT-2 and HCNT-3, respectively. Accordingly, the primary CNT fibers used to make these three electrodes

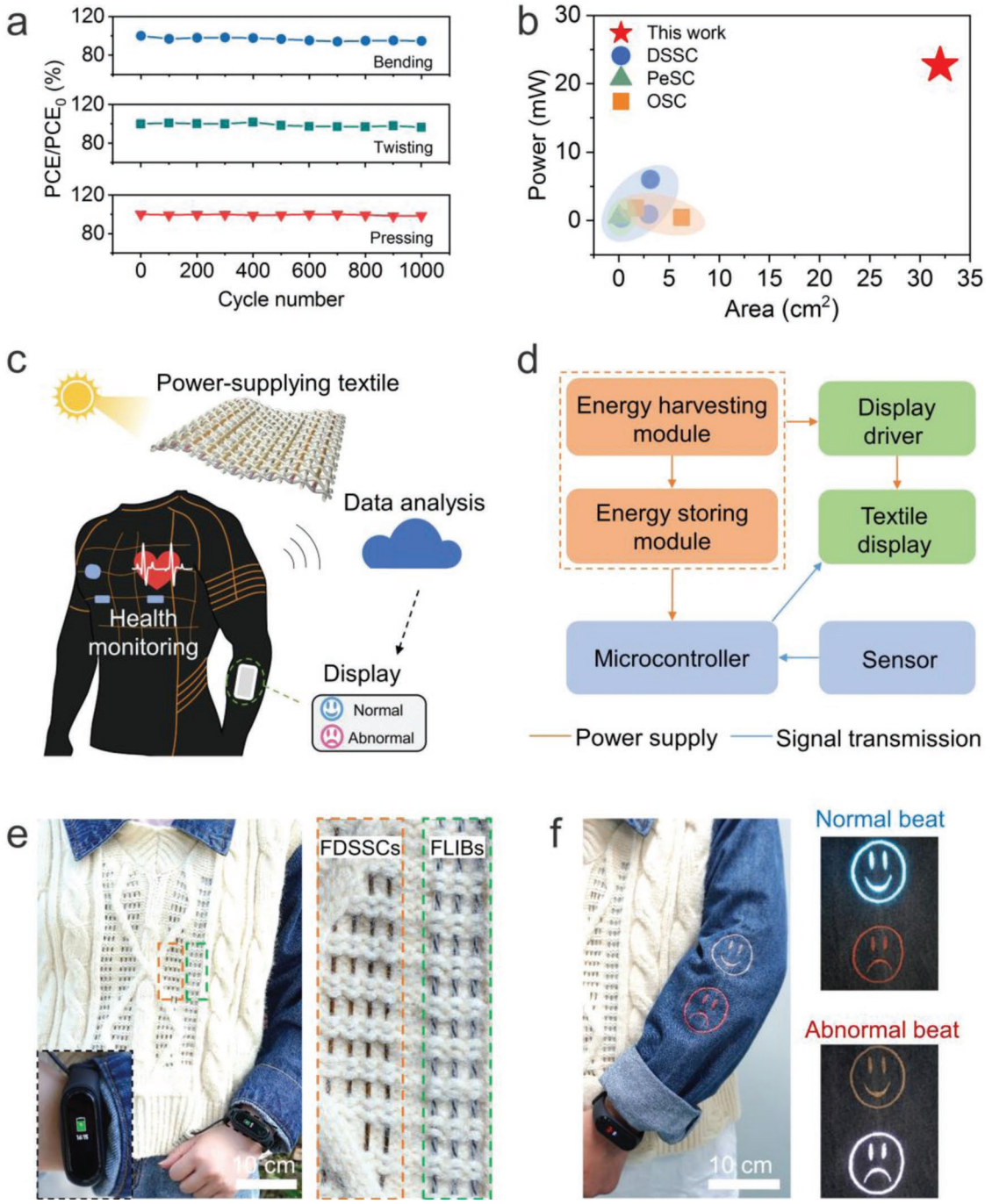

Figure 4. Application demonstrations of photovoltaic textiles. a) Variations of PCEs for FDSSCs after bent repeatedly (with bending angle of 120°), twisted (with a pitch of 4 cm and curvature radius of 0.5 cm), and pressed (with a pressure of 278 N m^{-2}). b) Comparison of the area and P_{max} of FDSSCs in the photovoltaic textile.[35–40] c) Schematic showing a smart healthcare garment integrated with self-powered textile, health monitoring and displaying modules. d) Diagram showing the integration design of smart garment. Health monitoring and displaying modules are powered by power-supplying textile. e) Photograph of a sweater integrated with FDSSCs and FLIBs charging a smart watch. f) Photograph showing textile display on the left arm powered by FDSSCs and FLIBs acting as an indicator of heart rate status.

were 60, 40 and 20 µm in diameter to ensure the overall diameter of the HCNT was consistent. Their SEM images were shown in Figures S18, S2, and S19 (Supporting Information), respectively; statistical distribution of microchannel sizes was summarized in Figure S20 (Supporting Information). Their average microchannel sizes were 3, 1.7 and 0.5 µm, respectively. Figure S21 (Supporting Information) depicted *J–V* curves of the FDSSCs made by the three fibers, indicating the highest photovoltaic performance of the HCNT-2. Therefore, the HCNT-2 fibers were used unless otherwise specified in the following study. Third, the HCNT fiber was immersed in 1 mM K_2PtCl_6 and 0.1 M KCl solution using platinum wire as the counter electrode to electrodeposit Pt by double potential step method (10 s at 0.5 V and –0.7 V terminated at 0.2 C), and then

they were collected on the reels. To investigate the effect of hierarchical channel structure on performance, the CNT fiber with the diameter of 150 µm was used as control group. The carbon fiber was purchased from Taiwan Carbon Technology Co., Ltd. (W0S1009).

Fabrication of Fiber Dye-Sensitized Solar Cells: The photoanode fibers were prepared from titanium wires modified with titanium dioxide nanotube arrays via an anodic oxidation method at 60 V for 6 h. The morphology of the fiber photoanode was shown in Figure S22 (Supporting Information). After annealing at 500 °C for 60 min in furnace, the Ti wire was immersed in 0.1 mM Y123 solution containing a mixture solvent of dehydrated acetonitrile and tert-butanol (1/1, v/v) for 16 h at least. The Y123 was selected due to its matched energy level with $Co^{2+/3+}$ and appropriate energy gap.[25] The as-prepared dye-absorbed Ti/TiO_2 wire was twisted with the counter electrode and then inserted into a flexible and transparent fluorinated ethylene propylene tube with an inner diameter of 600 µm and an outer diameter of 1000 µm. Then the Co^{2+}/Co^{3+} redox electrolyte was injected in the tube with a syringe.

Fabrication of Lithium-Ion Batteries and Textile Display Modules: Al wire (diameter of 200 µm) was used as positive electrode substrate, which was coated with the positive slurry (lithium cobalt oxide, super-P, polyvinylidene fluoride, *N*-methyl-2-pyrrolidone). And Cu wire (diameter of 200 µm) was used negative electrode substrate, which was coated with the negative slurry (graphite, super-P, sodium carboxymethyl cellulose, butadiene styrene rubber, water). The optimized loading weights of lithium cobalt oxide and graphite were 170 and 94 mg m^{-1}, respectively. The negative fiber was wrapped in separator strips and twisted with positive fiber. Then the electrodes were inserted into the encapsulation tube and injected with electrolyte. The textile display module was fabricated by sewing electroluminescent yarns. The electroluminescent yarns were prepared by twisting copper yarns (diameter of 100 µm) with stainless steel yarns (diameter of 200 µm) coated with ZnS slurry. The ZnS slurry was made by dispersing 75 wt.% ZnS phosphors in waterborne polyurethane.

Fabrication of Power-Supplying Textile: The energy harvesting module consisted of twelve FDSSCs, in which six FDSSCs were connected in series as a group, and the two groups were connected in parallel. The energy storing module consisted of three fiber lithium-ion batteries connected in series. The conducive Cu wires were used as the electrical connections for these two modules.

Characterization and Electrochemical Measurement: Surface morphologies and primary channel sizes were characterized by scanning electron microscopy (SEM, Carl Zeiss). Secondary channel sizes were characterized by N_2 absorption-desorption isotherms measured at 77 K on ASAP 2460 (Micromeritics). Keithley 2400 source meter was used to record *J–V* curves of FDSSCs under illumination of AM1.5 simulated solar light. To prevent surrounding interference, the FDSSC was placed on a black plate, and covered with black masks at both sides (Figure S23, Supporting Information). The light density at the surface of FDSSCs was calibrated by a standard silicon solar cell (Oriel-91150). The PCE was calculated by the following equation, $PCE = \frac{V_{oc} I_{sc} FF}{P_{in} A}$, where A represents the area of incident light, which is equal to the projection area of photoanode, and thus calculated by multiplying length by diameter of the photoanode.[42,56] The IPCE was measured by a Newport-74125 system. The electrochemical activity area was measured by cyclic voltammetry (CV) in 20 mM $K_4Fe(CN)_6$ and 0.2 M KCl at 20 mV s^{-1} with Ag/AgCl electrode, Pt, and as-prepared electrode as reference, counter, and working electrode, respectively. The normalized area was obtained by dividing the active area based on Randles-Sevcik Equation[34] by the surface area of electrode (0.0471 cm^2). The CV measurement toward Co^{2+}/Co^{3+} was carried out in the same three electrode system at a scan rate of 50 mV s^{-1}. Electrochemical impedance spectroscopy (EIS) was measured from 0.1 Hz to 100 kHz with AC amplitude of 10 mV. All CV and EIS measurement were performed at an electrochemical workstation. The experiments concerned with the wrist of human conformed to the regulation of Animal and Human Experimentation Committee of Fudan University. A healthy subject from Fudan University had provided written, informed consent before participating in the study.

Statistical Analysis: The sample number for statistical distribution of channel size was 50. And the average sizes for microchannels were presented as the mean ± standard deviation.

Supporting Information

Supporting Information is available from the Wiley Online Library or from the author.

Acknowledgements

X.K. and Z.Z. contributed equally to this work. This work was supported by NSFC (T2222005, 22175042, 52122310, 22075050, 52222310) and STCSM (20JC1414902, 21511104900).

Conflict of Interest

The authors declare no conflict of interest.

Data Availability Statement

The data that support the findings of this study are available in the supplementary material of this article.

Keywords

solar cells, carbon nanotube, fiber, textiles, wearable electronics

Received: July 7, 2022
Revised: September 17, 2022
Published online: October 13, 2022

[1] Z. Z. Zhao, C. Yan, Z. X. Liu, X. L. Fu, L. M. Peng, Y. F. Hu, Z. J. Zheng, *Adv. Mater.* **2016**, *28*, 10267.
[2] A. Libanori, G. R. Chen, X. Zhao, Y. H. Zhou, J. Chen, *Nat. Electron.* **2022**, *5*, 142.
[3] T. Lv, Y. Yao, N. Li, T. Chen, *Nano Today* **2016**, *11*, 644.
[4] L. Kou, T. Q. Huang, B. N. Zheng, Y. Han, X. L. Zhao, K. Gopalsamy, H. Y. Sun, C. Gao, *Nat. Commun.* **2014**, *5*, 3754.
[5] G. Wang, J. Zhang, C. Yang, Y. Wang, Y. Xing, M. A. Adil, Y. Yang, L. Tian, M. Su, W. Shang, K. Lu, Z. Shuai, Z. Wei, *Adv. Mater.* **2020**, *32*, 2005153.
[6] W. J. Xu, S. T. Wu, X. M. Li, M. C. Zou, L. S. Yang, Z. L. Zhang, J. Q. Wei, S. Hu, Y. H. Li, A. Y. Cao, *Adv. Energy Mater.* **2016**, *6*, 1600095.
[7] M. D. Ye, X. R. Wen, M. Y. Wang, J. Iocozzia, N. Zhang, C. J. Lin, Z. Q. Lin, *Mater. Today* **2015**, *18*, 155.
[8] G. R. Chen, Y. Z. Li, M. Bick, J. Chen, *Chem. Rev.* **2020**, *120*, 3668.
[9] Y. K. Zhang, S. W. Ng, X. Lu, Z. J. Zheng, *Chem. Rev.* **2020**, *120*, 2049.
[10] R. Y. Liu, Z. L. Wang, K. Fukuda, T. Someya, *Nat. Rev. Mater.* **2022**, s41578, https://doi.org/10.1038/s41578-022-00441-0.
[11] H. Sun, Y. Zhang, J. Zhang, X. M. Sun, H. S. Peng, *Nat. Rev. Mater.* **2017**, *2*, 17023.
[12] M. Hatamvand, E. Kamrani, M. Lira-Cantu, M. Madsen, B. R. Patil, P. Vivo, M. S. Mehmood, A. Numan, I. Ahmed, Y. Q. Zhan, *Nano Energy* **2020**, *71*, 104609.

[13] W. J. Ma, Y. Zhang, S. W. Pan, Y. H. Cheng, Z. Y. Shao, H. X. Xiang, G. Y. Chen, L. P. Zhu, W. Weng, H. Bai, M. F. Zhu, *Chem. Soc. Rev.* **2021**, *50*, 7009.
[14] C. S. Huang, S. Yakunin, J. Avaro, X. Y. Kang, M. I. Bodnarchuk, M. Liebi, X. M. Sun, R. M. Rossi, M. V. Kovalenko, L. F. Boesel, *Adv. Energy Mater.* **2022**, *12*, 2200441.
[15] J. Liang, G. Zhu, C. Wang, Y. Wang, H. Zhu, Y. Hu, H. Lv, R. Chen, L. Ma, T. Chen, Z. Jin, J. Liu, *Adv. Energy Mater.* **2017**, *7*, 1601208.
[16] Z. Yang, J. Deng, X. Sun, H. Li, H. Peng, *Adv. Mater.* **2014**, *26*, 2643.
[17] Z. Yang, H. Sun, T. Chen, L. Qiu, Y. Luo, H. Peng, *Angew. Chem. Int. Ed.* **2013**, *52*, 7545.
[18] S. N. Yun, A. Hagfeldt, T. L. Ma, *Adv. Mater.* **2014**, *26*, 6210.
[19] X. Q. Liu, J. Iocozzia, Y. Wang, X. Cui, Y. H. Chen, S. Q. Zhao, Z. Li, Z. Q. Lin, *Energy Environ. Sci.* **2017**, *10*, 402.
[20] L. Chen, H. Yin, Y. Zhou, H. Dai, T. Yu, J. Liu, Z. Zou, *Nanoscale* **2016**, *8*, 2304.
[21] A. Ali, S. M. Shah, S. Bozar, M. Kazici, B. Keskin, M. Kaleli, S. Akyurekli, S. Gunes, *Nanotechnology* **2016**, *27*, 384003.
[22] X. Fu, H. Sun, S. Xie, J. Zhang, Z. Pan, M. Liao, L. Xu, Z. Li, B. Wang, X. Sun, H. Peng, *J. Mater. Chem. A* **2018**, *6*, 45.
[23] S. N. Yun, Y. F. Liu, T. H. Zhang, S. Ahmad, *Nanoscale* **2015**, *7*, 11877.
[24] L. Giribabu, R. Bolligarla, M. Panigrahi, *Chem. Rec.* **2015**, *15*, 760.
[25] J. Wu, Z. Lan, J. Lin, M. Huang, Y. Huang, L. Fan, G. Luo, *Chem. Rev.* **2015**, *115*, 2136.
[26] Z. Li, Z. Liu, H. Y. Sun, C. Gao, *Chem. Rev.* **2015**, *115*, 7046.
[27] L. Yao, Q. Wu, P. X. Zhang, J. M. Zhang, D. R. Wang, Y. L. Li, X. Z. Ren, H. W. Mi, L. B. Deng, Z. J. Zheng, *Adv. Mater.* **2018**, *30*, 1706054.
[28] H. Zhang, W. Q. Zhao, M. C. Zou, Y. S. Wang, Y. J. Chen, L. Xu, H. S. Wu, A. Y. Cao, *Adv. Energy Mater.* **2018**, *8*, 1800013.
[29] X. T. Meng, C. Yu, X. D. Song, J. Iocozzia, J. F. Hong, M. Rager, H. L. Jin, S. Wang, L. L. Huang, J. S. Qiu, Z. Q. Lin, *Angew. Chem. Int. Ed.* **2018**, *57*, 4682.
[30] X. T. Meng, C. Yu, X. P. Zhang, L. L. Huang, M. Rager, J. F. Hong, J. Qiu, Z. Q. Lin, *Nano Energy* **2018**, *54*, 138.
[31] S. Mathew, A. Yella, P. Gao, R. Humphry-Baker, B. F. Curchod, N. Ashari-Astani, I. Tavernelli, U. Rothlisberger, M. K. Nazeeruddin, M. Gratzel, *Nat. Chem.* **2014**, *6*, 242.
[32] J. A. Baker, C. Worsley, H. K. H. Lee, R. N. Clark, W. C. Tsoi, G. Williams, D. A. Worsley, D. T. Gethin, T. M. Watson, *Adv. Eng. Mater.* **2017**, *19*, 1600652.
[33] L. Kavan, J. H. Yum, M. Gratzel, *Nano Lett.* **2011**, *11*, 5501.
[34] S. Hrapovic, Y. L. Liu, K. B. Male, J. H. T. Luong, *Anal. Chem.* **2004**, *76*, 1083.
[35] P. Lv, Y. Y. Feng, P. Zhang, H. M. Chen, N. Q. Zhao, W. Feng, *Carbon* **2011**, *49*, 4665.
[36] A. A. Shvedova, N. Yanamala, E. R. Kisin, A. V. Tkach, A. R. Murray, A. Hubbs, M. M. Chirila, P. Keohavong, L. P. Sycheva, V. E. Kagan, V. Castranova, *Am. J. Physiol. Lung Cell Mol. Physiol.* **2014**, *306*, 170.
[37] M. H. Sun, S. Z. Huang, L. H. Chen, Y. Li, X. Y. Yang, Z. Y. Yuan, B. L. Su, *Chem. Soc. Rev.* **2016**, *45*, 3479.
[38] Y. Li, Z.-Y. Fu, B.-L. Su, *Adv. Funct. Mater.* **2012**, *22*, 4634.
[39] A. Sacco, *Renewable Sustainable Energy Rev.* **2017**, *79*, 814.
[40] S. Sarker, A. J. S. Ahammad, H. W. Seo, D. M. Kim, *Int. J. Photoenergy* **2014**, *2014*, 851705.
[41] M. Peng, D. C. Zou, *J. Mater. Chem. A* **2015**, *3*, 20435.
[42] R. E. A. Ardhi, M. X. Tran, M. X. Wang, G. C. Liu, J. K. Lee, *J. Mater. Chem. A* **2020**, *8*, 2549.
[43] T. Stergiopoulos, P. Falaras, *Adv. Energy Mater.* **2012**, *2*, 616.
[44] G. Liu, M. Wang, H. Wang, R. E. A. Ardhi, H. Yu, D. Zou, J. K. Lee, *Nano Energy* **2018**, *49*, 95.
[45] G. Liu, M. Peng, W. Song, H. Wang, D. Zou, *Nano Energy* **2015**, *11*, 341.
[46] H. Sun, X. You, J. E. Deng, X. L. Chen, Z. B. Yang, J. Ren, H. S. Peng, *Adv. Mater.* **2014**, *26*, 2868.
[47] S. Casadio, N. Sangiorgi, A. Sangiorgi, A. Dessì, L. Zani, M. Calamante, G. Reginato, A. Mordini, A. Sanson, *Sol. Energy Mater. Sol. Cells* **2021**, *224*, 110986.
[48] C.-S. Huang, X. Kang, R. M. Rossi, M. V. Kovalenko, X. Sun, H. Peng, L. F. Boesel, *J. Mater. Chem. A* **2021**, *9*, 25974.
[49] D. Lv, Q. Jiang, Y. Shang, D. Liu, *npj Flexible Electron.* **2022**, *6*, 38.
[50] M. Peng, K. Yan, H. Hu, D. Shen, W. Song, D. Zou, *J. Mater. Chem. C* **2015**, *3*, 2157.
[51] P. Liu, Z. Gao, L. Xu, X. Shi, X. Fu, K. Li, B. Zhang, X. Sun, H. Peng, *J. Mater. Chem. A* **2018**, *6*, 19947.
[52] B. Dong, J. Hu, X. Xiao, S. Tang, X. Gao, Z. Peng, D. Zou, *Adv. Mater. Technol.* **2019**, *4*, 1900131.
[53] M. Liao, C. Wang, Y. Hong, Y. Zhang, X. Cheng, H. Sun, X. Huang, L. Ye, J. Wu, X. Shi, X. Kang, X. Zhou, J. Wang, P. Li, X. Sun, P. Chen, B. Wang, Y. Wang, Y. Xia, Y. Cheng, H. Peng, *Nat. Nanotechnol.* **2022**, *17*, 372.
[54] X. Shi, Y. Zuo, P. Zhai, J. H. Shen, Y. Y. W. Yang, Z. Gao, M. Liao, J. X. Wu, J. W. Wang, X. J. Xu, Q. Tong, B. Zhang, B. J. Wang, X. M. Sun, L. H. Zhang, Q. B. Pei, D. Y. Jin, P. N. Chen, H. S. Peng, *Nature* **2021**, *591*, 240.
[55] S. M. Feldt, E. A. Gibson, E. Gabrielsson, L. Sun, G. Boschloo, A. Hagfeldt, *J. Am. Chem. Soc.* **2010**, *132*, 16714.
[56] M. R. Lee, R. D. Eckert, K. Forberich, G. Dennler, C. J. Brabec, R. A. Gaudiana, *Science* **2009**, *324*, 232.